Updated Models of Current Sheet and Magnetic Field in the Jovian Magnetosphere for Pre-Galileo, Galileo and Juno Eras

Naoya Momoki[1] and Hiroaki Toh[2]

[1]Division of Earth and Planetary Sciences, Graduate School of Science, Kyoto University
[2]Graduate School of Science, Kyoto University

November 22, 2022

Abstract

In Jupiter's magnetosphere, an electric current system within the 'current sheet' generates a magnetic field, which is comparable to or dominating the Jovian intrinsic field in the magnetosphere. However, update of an existing model of the magnetospheric field by Khurana (1997) using newly acquired data by Galileo and Juno has never been conducted since it was first formulated. Here we used the data by Voyager 1/2, Galileo and Juno to revise the current sheet shape model as well as the magnetospheric field model based on each spacecraft data. We derived fits that reproduced each data well, and revealed long-term variations of both current sheet and magnetospheric field over several decades. The updated models could be useful for detecting dynamic events in the magnetosphere such as magnetopause deformation and plasmoid generation. They can also be used as external fields necessary for probing into the Galilean icy moons by electromagnetic induction methods.

Hosted file

essoar.10511021.1.docx available at https://authorea.com/users/539778/articles/600014-updated-models-of-current-sheet-and-magnetic-field-in-the-jovian-magnetosphere-for-pre-galileo-galileo-and-juno-eras
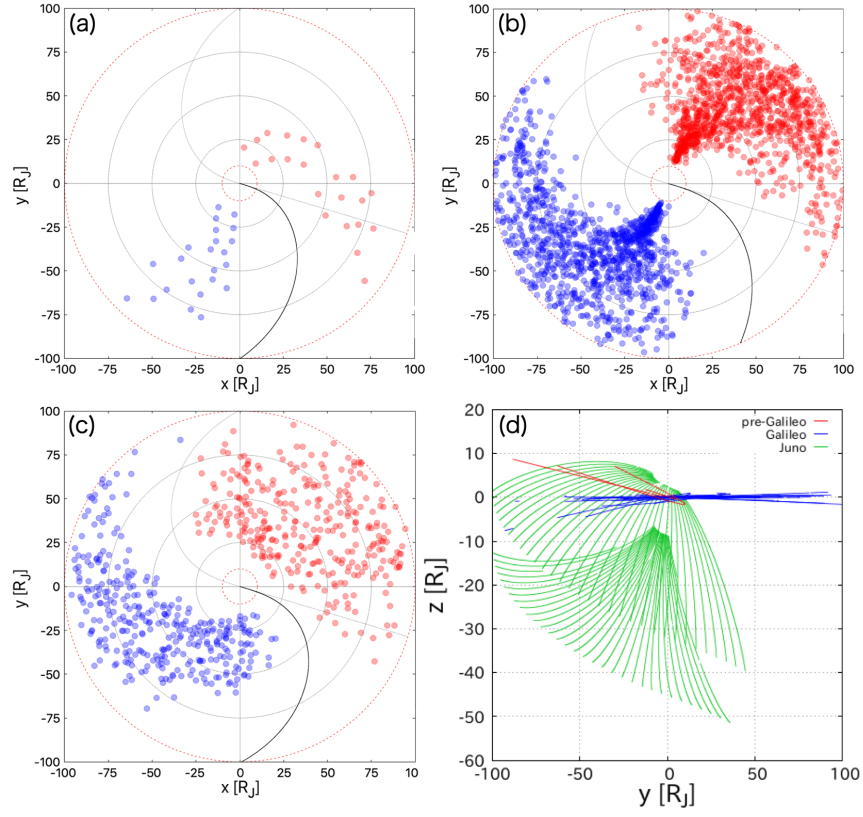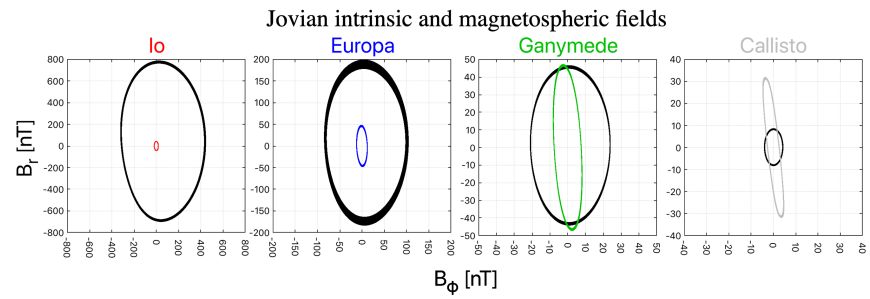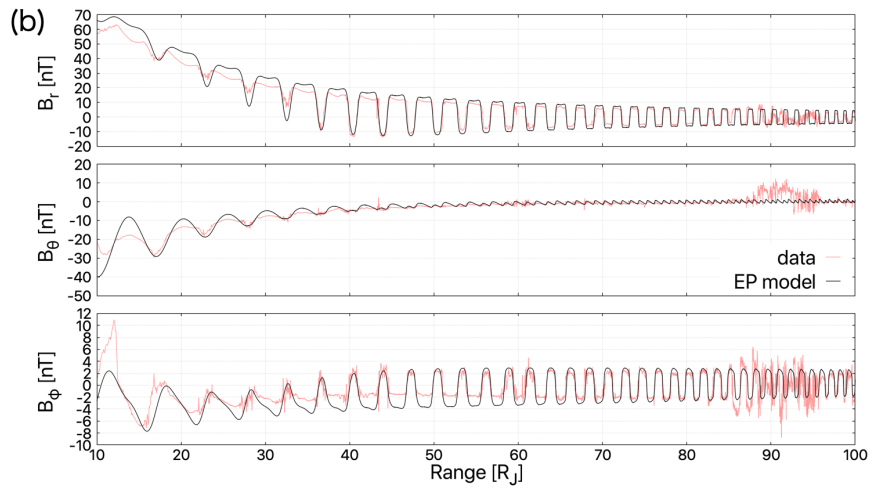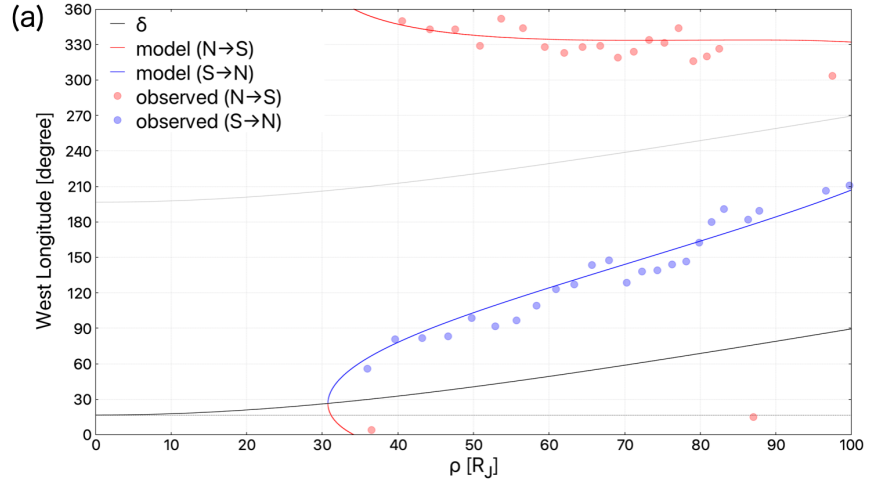
2

Jovian intrinsic and magnetospheric fields

Naoya Momoki[1] and Hiroaki Toh[2]

[1] Division of Earth and Planetary Sciences, Graduate School of Science, Kyoto University

[2] Data Analysis Center for Geomagnetism and Space Magnetism, Graduate School of Science, Kyoto University

Corresponding author: Hiroaki Toh (tou.hiroaki.7u@kyoto-u.ac.jp)

Key Points:

- We updated existing models of both current sheet and magnetic field in the Jovian magnetosphere using pre-Galileo, Galileo and Juno data.

- Differences among the updated models may represent long-term variations of the current system in the Jovian magnetosphere.

- The models are useful for study on magnetospheric dynamics and prediction of temporal magnetic variations external to Galilean icy moons.

Abstract

In Jupiter's magnetosphere, an electric current system within the 'current sheet' generates a magnetic field, which is comparable to or dominating the Jovian intrinsic field in the magnetosphere. However, update of an existing model of the magnetospheric field by Khurana (1997) using newly acquired data by Galileo and Juno has never been conducted since it was first formulated. Here we used the data by Voyager 1/2, Galileo and Juno to revise the current sheet shape model as well as the magnetospheric field model based on each spacecraft data. We derived fits that reproduced each data well, and revealed long-term variations of both current sheet and magnetospheric field over several decades. The updated models could be useful for detecting dynamic events in the magnetosphere such as magnetopause deformation and plasmoid generation. They can also be used as external fields necessary for probing into the Galilean icy moons by electromagnetic induction methods.

Plain Language Summary

Above Jupiter's atmosphere and ionosphere, there is a vast region coined 'magnetosphere' where magnetic fields govern physical phenomena. The magnetic fields in the magnetosphere are divided mainly into two components: one arising from inside Jupiter, and the other generated by electric currents flowing in a current sheet in the magnetosphere. Although both had been modeled so far, the models are, as usual, not perfect and should be updated on arrival of new datasets. Unfortunately, one of the models of the magnetospheric field is especially far from up to date, compared with the intrinsic field. In this study, we focused on the magnetospheric field and its associated current sheet shape models using three datasets by four spacecraft, pre-Galileo (Voyager 1 and Voyager 2), Galileo and Juno. By updating the models for each dataset, we determined three pairs of current sheet shape and magnetospheric field that

1

showed long-term variations of Jupiter's magnetosphere over nearly half a century. The three pairs could be useful to detect dynamic events in the Jovian magnetosphere such as temporal changes of its shape and coherent plasma releases, and for probing deep into the Galilean icy moons that are thought to be possible cradles of extraterrestrial lives.

1 Introduction

The Jovian magnetosphere has been probed by several spacecraft and thus vector magnetic data have also been accumulated intermittently. Since the first flyby to Jupiter by Pioneer 10 in 1973, six spacecraft (Pioneer 11, Voyager 1, Voyager 2, Ulysses, Cassini and New Horizons) flew by and five out of them (without New Horizons) conducted magnetic observations. Galileo was the very first orbiter inserted into Jovicentric orbits, and now Juno is in Jupiter's polar orbits. One of the main applications of the magnetic data is modeling of the Jovian magnetic field,which mainly consists of the Jovian intrinsic and magnetospheric magnetic fields.

The Jovian intrinsic field is originated from the dynamo action inside Jupiter. Its models have been studied intensively since the first observation by Pioneer 10, e.g., Smith et al. (1974), O_6 (Connerney, 1992), VIP4 (Connerney et al., 1998), VIT4 (Connerney, 2007), VIPAL (Hess et al., 2011), Ridley and Holme (2016), JRM09 (Connerney et al., 2018) and JRM33 (Connerney et al., 2021). On the other hand, the magnetospheric field is originated from electric current systems outside Jupiter such as current sheet (CS) and magnetopause currents, and its models have been studied by fewer reseachers (e.g., Alexeev & Belenkaya, 2005; Connerney et al., 1981; Khurana, 1997). Updates of the models using new data by Galileo and/or Juno are limited (e.g., Connerney et al., 2020; Khurana, 2001; Khurana & Schwarzl, 2005; Lorch et al., 2020; Russel et al., 2001; Vogt et al., 2017; Wang et al., 2022) and have not caught up with the accumulation of the data. Nevertheless, the magnetospheric field models have a wide range of applications such as predicting the magnetic field that a spacecraft may observe (e.g. Kivelson et al., 1997), calculating the magnetic field external to Jupiter's satellites for electromagnetic (EM) induction studies (e.g. Khurana et al., 2009) and so on.

We adopted the combined formulation of the magnetospheric field by Khurana (1997) and the shape of the CS by Khurana (1992) in this study. First, we updated the CS shape model parameters for each dataset by Galileo and Juno in addition to the pre-Galileo spacecraft (Voyager 1 and 2) as described in the next section. We then redetermined Euler potentials (Stern, 1970, 1976) of the magnetospheric field to investigate the possible long-term variation of the CS shape and the magnetospheric field by comparing the three sets of updated models. The newly updated models have a wide range of application such as detecting magnetospheric dynamic phenomena associated with magnetotail reconnections and magnetopause variations. They are also capable of prediction of inducing fields at each Galilean icy moon for EM induction purposes. The new models are of use for the future missions, JUICE and Europa Clipper, as

well in order to estimate the magnetospheric field along their trajectories.

2 Models

Khurana's (1997) model that we adopted in this study is an Euler potential model of the magnetic field generated by electric currents flowing within the CS of the magnetosphere. The shape of the CS varies with Jupiter's rotation and is influenced by the shape of the magnetosphere (Khurana & Kivelson, 1989; Northrop et al., 1974). It is also necessary to model it as a function of time, or local time before deriving the Euler potentials as had been done by Khurana (1992).

$$
\begin{aligned}
Z_{\mathrm{CS}} &= \rho \tan\left(\theta_d\right) \frac{x_0}{x} \tanh\left(\frac{x}{x_0}\right) \cos(\lambda - \delta) \\
\delta &= \lambda_d + \frac{\Omega_J \rho_0}{v_0} \ln \cosh\left(\frac{\rho}{\rho_0}\right)
\end{aligned}
\#(\ SEQ\ Equation\ \backslash * \ ARABIC\ 1)
$$

The CS shape model adopted here is characterized by the following three parameters: (x_0, ρ_0, v_0). An advantage of Khurana's (1992) model is that it can replicate two features of the CS that were revealed by past observations, namely, bendback and hinge, which are controlled by the parameters (detailed explanations are in Supporting Information). The bendback is an effect that the CS distorts westward with the increasing ρ, and manifests in δ. While this effect is non-axisymmetric in general (Khurana & Scgwarzl, 2005), it is assumed axisymmetric in his original formulation. It is caused by the finite propagation velocity of the tilted magnetic dipole oscillation associated with Jupiter's rotations and/or the non-corotating plasmas in the middle and the outer magnetosphere (Khurana, 1997; Northrop et al., 1974). On the other hand, the hinge is a non-axisymmetric effect that the Z_{CS} is saturated by the solar wind, and thus a strong function of x. While the bendback results in delayed CS encounters of a spacecraft (Northrop et al., 1974) compared with a rigid CS plane (i.e., no both effects), the hinge promotes earlier encounters in some cases. When a spacecraft is located in the north of the Jovigraphic equator, the hinged CS results in delayed encounters when the spacecraft crosses the CS from north to south. However, earlier encounters occur at the time of south to north crossings (Bridge et al., 1979; Ness et al., 1979).

$$
\begin{aligned}
\mathbf{B} &= f \times g \\
f &= -C_1 \rho_m \left[\tanh\left(\frac{r_{01}}{r}\right)\right]^{a_1} \ln \cosh\left(\frac{Z_m - Z_{m,CS}}{D_1}\right) \\
&\quad + \int \rho_m \left\{ C_2 \left[\tanh\left(\frac{\rho_{02}}{\rho_m}\right)\right]^{a_2} + C_3 \left[\tanh\left(\frac{\rho_{03}}{\rho_m}\right)\right]^{a_3} + C_4 \right\} d\rho_m \\
g &= \phi + p \left[1 + q\ \tanh^2\left(\frac{Z_m - Z_{m,CS}}{D_2}\right)\right] \rho_m
\end{aligned}
\#(\ SEQ\ Equation\ \backslash * \ ARABIC
$$

In the previous studies, the data by Pioneer 10, Voyager 1 and Voyager 2 were used to determine the seventeen parameters above. When constructing these models, a Jovian intrinsic field model was necessary, and in this study

we adopted the JRM09 model based on the Juno data . Although the secular variations of the intrinsic field may present (Moore et al, 2019; Ridley & Holme, 2016; Yu et al, 2010), it is thought to be a few percents of the total field for the time interval considered here and confined to local regions (e.g., Fig. 4 of Moore et al., 2019), and we applied the model to all the spacecraft data. This means that we neglected the secular variation of the intrinsic field in the distant region we are addressing.

3 Data

In this study, we used the vector magnetic data by Voyager 1/2, Galileo and Juno available at NASA's PDS. As for Juno, data from the initial 23 orbits and the first half of the 24th orbit were used. Following the previous studies, we adopted the data at Jovicentric distances from 10 to 100 R_J ($1R_J$=71,492km) and in the nightside (from 1800 to 0600 LT).

We updated the models by optimizing their parameters including the new data. For the CS shape model, we determined the three parameters by fitting the estimated positions of the CS defined by B_r reversals. For the magnetospheric field model, we updated the 14 parameters by fitting the observed magnetic field data to Eq. (2).

Because the range of possible crossing latitudes are nearly equal to that of dipole equator latitudes, we restricted the latitude of the data in addition to the constraints on the Jovicentric distance and the local time. Specifically, we adopted the data within the Jovicentric latitudes of $\pm 10.31°$ corresponding to the θ_d of the JRM09 model.

We can find the CS crossings by zero radial components (B_r= 0) of the magnetic field data. To pick up the crossings, we first took 60 minutes running averages of the data and identified the zero radial components in the smoothed data as candidates for the crossings. Then, we selected a final set of the crossings by imposing two constraints on the candidates: (1) cadense of the crossings and (2) coincidence with minima of the magnetic field strength data. The two crossings per Junpiter's rotation are expected to occur at relatively low latitudes associated because of the non-zero θ_d. Taking advantage of this scenario, we excluded non-periodic candidates. Since we can reasonably assume that in the steady state, the pressure in the CS balances that in the lobe (Lanzerotti et al., 1980), we can expect that minima of the magnetic field strength coincide with the crossings. Using this rule of thumb, we excluded candidates that lose clear correlation with the field strength. Thanks to the two constraints, we succeeded in extracting reliable CS crossings for use in the subsequent model updates. The time resolutions of the data are 48-second for Voyager 1/2, typically 24-second for Galileo, and 1-second for Juno. While Voyager's resolution may make an error of ~0.5 degree in longitude, this error is relatively small compared with fitting RMSs listed in Table 1 below. We, therefore, regarded that the differences in sampling rates can be ignored.

For the magnetospheric field model, we consider the observed magnetic data

as a sum of the Jovian intrinsic and magnetospheric field. In addition, magnetospheric fields by current systems other than in the CS itself are assumed small enough within the region of the magnetosphere of this study. Under these assumptions, we determined the observed magnetospheric field as vector deviations from the intrinsic field model (JRM09).

4 Methods

Following the previous studies, we updated the models in two steps. First, we determined the three parameters of the CS shape model based on Khurana (1992). Second, we estimated the fourteen parameters of the magnetospheric field model based on Khurana (1997) by fixing the CS shape parameters as known constants, instead of determining all the paramters simultaneously. We reorganized the magnetic data by four spacecraft into three datasets, pre-Galileo (Voyager 1 and 2), Galileo and Juno, and updated the models for each dataset so that we may find long-term variations of the CS shape and/or the field, if any, by comparing the three.

As a method of optimization, we adopted a least square method with a gradient search technique. While the technique can find a local minimum, it is not guaranteed that the detected minimum is the global minimum. To circumvent the difficulty, we optimized the parameters from 125 initial parameter sets for the CS shape model and 100 initial sets for the magnetospheric field model.

$$\lambda_{\mathrm{model}} \quad = \quad \delta_{\mathrm{data}} \pm \cos^{-1}\left\{ Z_{CS,data}\left[\rho_{\mathrm{data}}\tan\left(\theta_d\right)\frac{x_0}{x_{\mathrm{data}}}\tanh\left(\frac{x_{\mathrm{data}}}{x_0}\right)\right]^{-1}\right\}, \#(\textit{ SEQ Equation } \backslash * \textit{ ARABIC 4}$$

For calculating the RMSs necessary for the magnetospheric field model, we used all the three components of the modeled and the observed magnetic field.

5 Results

The CS crossings detected by the method mentioned in the previous section are shown in Figure 1. The numbers of the crossings are 45 for pre-Galileo, 2283 for Galileo and 657 for Juno, which are mainly dependent on each spacecraft's trajectory. The updated model parameters of the CS shape are listed in Table 1 together with RMSs in addition to those of Khurana (1992). Although we updated them with the method different from that of Khurana (1992), the determined parameters of the pre-Galileo model (especially x_0 and v_0 that are not affected significantly by the choice of the intrinsic model) are consistent with those of Khurana (1992)
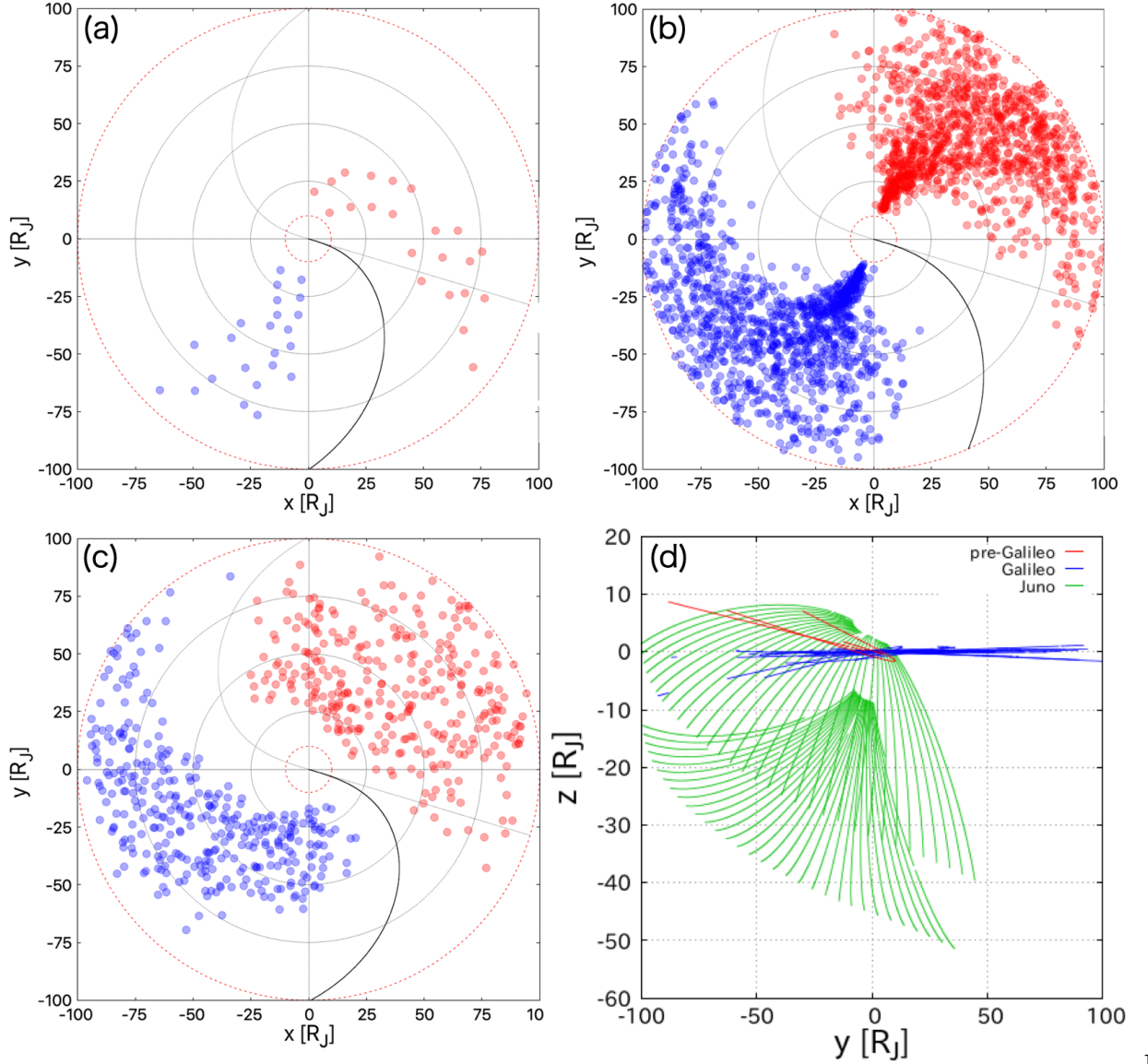
1. (a)–(c) Distribution of the crossings observed by Voyager 1/2, Galileo and Juno, respectively, projected on the Jovigraphical equator with the System III prime meridian as x-axis. The coordinates are measured in units of R_J. Red circles represent north-to-south crossings while blue ones correspond to south-to-north crossings. Red dashed circles represent the distance range of the used data. Black and gray curves denote δ and $\delta + 180°$. (d) Trajectories of each spacecraft within the same distance range, projected on the y-z plane of the Jupiter de-Spun Sun coordinate system. Both coordinates are measured in units of R_J. Red, blue and green lines represent the trajectories of Voyager

1/2, Galileo and Juno, respectively.
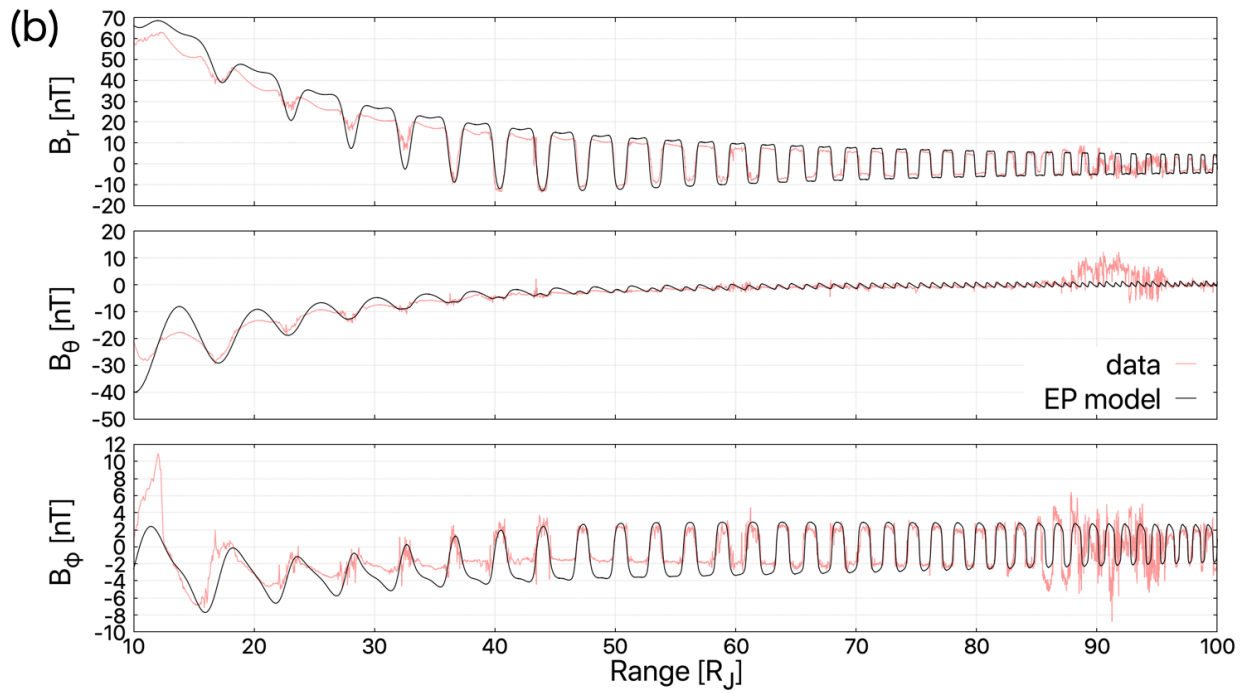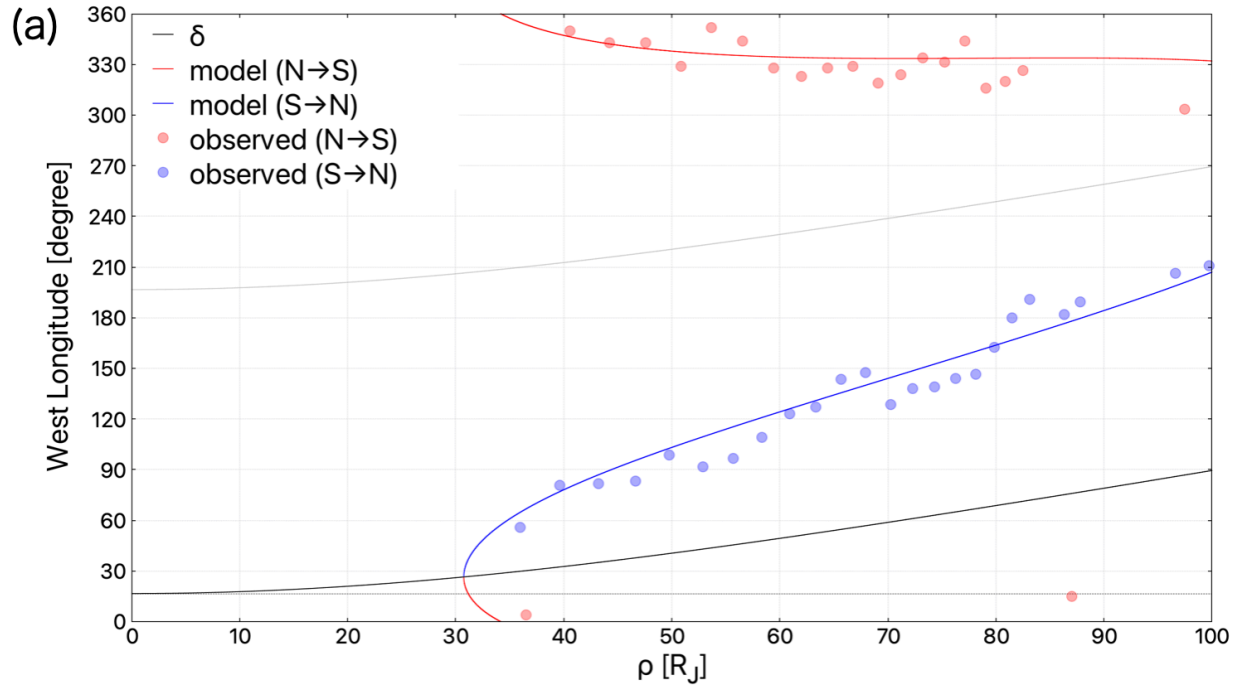
Figure 2. Comparison of the model predictions and the data on the inbound trajectory of the Juno peri-06. (a) The CS crossing data (circles) and the updated CS (lines) in System III coordinates for $10\ R_J < \rho < 100\ R_J$. The red circles and line indicate the north-to-south crossings, while the south-to-north results are shown in blue. Black and gray curves represent δ and $\delta + 180°$. (b) The magnetospheric field (observation minus JRM09) by Juno (red) and the modeled field (black) in System III coordinates for $10\ R_J < r < 100\ R_J$. The top, middle and bottom panels show B_r, B_θ and B_ϕ in nT, respectively.

model, which demonstrates validity of our method for updates. An example of the comparison between the detected crossings and the modeled CS is shown in Figure 2a. The detected crossings show two features: (1) the westward shift with the increasing ρ by the bendback and (2) the proximity to δ or $\delta + 180°$ by the hinge and/or spacecraft's migration into high latitudes, and the model reproduces these two well. Although it is the average model using all the data from the full mission period each, Fig. 2a indicates that it is useful for the prediction of the crossings at each orbit.

The updated model parameters of the magnetospheric field and RMSs are also listed in Table 1 together with those of Khurana's (1997) common model. Comparison of the magnetospheric magnetic data with the model predictions is shown in Figure 2b. B_r and B_ϕ show periodic variations associated with Jupiter's rotation and B_θ represents a northward magnetic field by eastward electric currents within the CS. The updated model fits the observed data well except for a fluctuation seen at around $90\ R_J$, which implies a possible detection of a

Table 1. The updated model paramters and their RMSs by pre-Galileo (Voyager 1/2), Galileo and Juno together with those by Khurana (1992, 1997) for both CS shape and magnetospheric field. The parameters of Khurana (1997) are those of the common model.

Current sheet	pre-Galileo	Galileo	Juno	Khurana (1992)
x_0	-36.1	-35.2	-43.5	33.5
ρ_0	14.9	29.2	49.9	33.2
v_0	44.5	58.9	33.0	37.4
RMS [degree]	10.5	22.0	19.1	11.2
Magnetic field	pre-Galileo	Galileo	Juno	Khurana (1997)
C_1	95.3	112.2	177.2	80.3
C_2	1852.5	874.6	61.1	690.4
C_3	-228.3	40.5	78.7	101.3
C_4	-1.4	-0.81	-0.79	-1.7
a_1	2.19	2.28	1.71	2.49
a_2	2.20	2.80	286.51	1.80
a_3	20.50	4.68	2.83	2.64
r_{01}	34.6	28.9	20.3	38.0
ρ_{02}	3.13	4.07	18.99	2.14

Current sheet	pre-Galileo	Galileo	Juno	Khurana (1992)
ρ_{03}	16.9	25.5	16.9	12.5
D_1	2.30	2.36	2.66	2.01
D_2	14.60	9.69	18.19	13.27
p	4.53	3.79	3.94	6.26
q	0.77	0.32	0.58	0.35
RMS [nT]	3.778	3.950	2.859	4.01

dynamic event in the pre-dawn magnetosphere. We will argue the implication of this in the next section. The comparison of the parameters between three models is in Figure S3 with the parameter errors based on the observation errors, which clearly indicates that there are significant variabilities for some parameters. Figures S4 through S6 represent the variations of the RMSs in the vicinity of the updated parameter values, and they guarantee the accuracy of the updates in this study.

6 Discussion

Differences of the bendback effect among the updated CS shape models can be estimated by v_0 values listed in Table 1 and Figure S1 showing the δ curves of each model in the Jovigraphic equatorial plane. The v_0 values whose reciprocals determine the bendback strength and the δ curves indicate a weak bendback of the Galileo model. Because v_0 corresponds to the Alfvén velocity that conveys Jupiter's rotation phase to the CS, the weak bendback of the Galileo model may imply a relatively large Alfvén velocity during the Galileo era. One concern is the difference in spacecraft's trajectories as well as the reported spatial dependence of the bendback (Khurana, 2001; Khurana & Schwarzl, 2005). We must be careful in distinguishing the detected changes from the spatial dependence of the CS in order to interpret it in terms of temporal variations.

The comparative study on $|x_0|$ values listed in Table 1 may reveal temporal variations of the hinge effect, which is also shown in Figure S2 in the form of meridional cross-sections of the CSs. The relatively large $|x_0|$ value and the maximum Z_{CS} of the cross-section indicates the weak hinge of the Juno model. Although the hinge can be strengthened by the compression of the magnetosphere with increasing solar wind dynamic pressure, it is difficult to know the actual solar wind parameters near Jupiter when a spacecraft is in the magnetosphere. One of the indices that correlates with the averaged dynamic pressure is the solar activity that manifests in the sunspot numbers (Jackman & Arridge, 2011). The solar activity is minimum in the Juno era, while it was close to maximum in both Voyager and Galileo eras, and this may explain the large maximum Z_{CS} found in this study through the averaged changes of the Jovian magnetopause
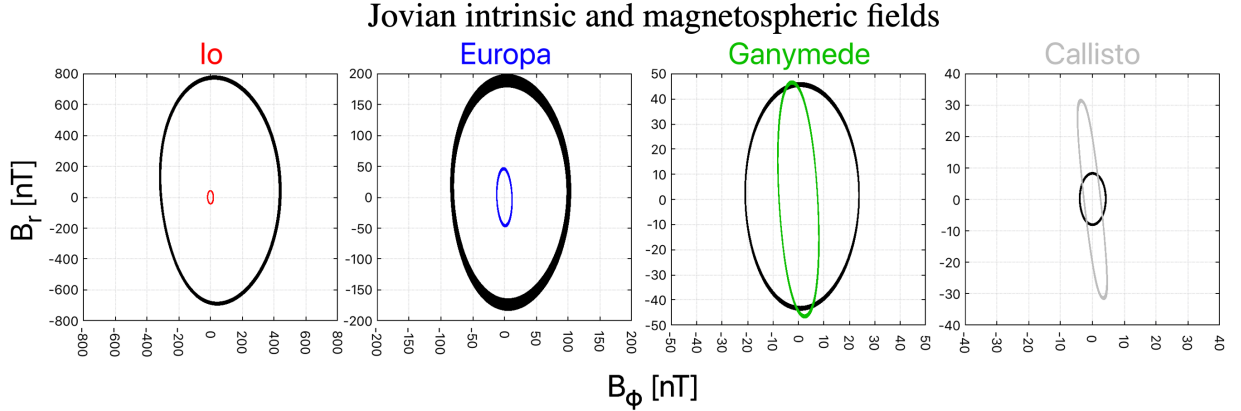
Figure 3. Hodograms of B_r and B_ϕ components of the intrinsic field (JRM09, black) and the updated magnetospheric field by Juno (other colors) at each Galilean satellite in nT.

position (e.g., Joy et al., 2002). The long-term variation of Z_{CS} has not been reported before and may imply that the influence of the solar wind can reach the low-latitude magnetosphere. However, the variation may also be influenced by the spacecrafts' trajectories, though they are beyond the scope of this study.

The electric current density generating the field can be calculated analytically by taking the rotation of Eq. (2). The azimuthal component of the electric current density calculated by Galileo and Juno models are shown in Figs. S7 and S8. The relatively high density region is more expanded in the Juno model than that in the Galileo model, which is consistent with the relatively weak bendback (large Alfvén velocity) in the Galileo era.

Magnetospheric magnetic data sometimes include irregular fluctuations. An example has already been shown in the Figure 2b near 90 R_J. These fluctuations are significant especially in the outer magnetosphere with smaller frequencies than that of the Jovian rotation. It, therefore, is natural to consider them being caused by magnetic reconnections in the magnetotail or spacecraft's magnetopause crossings. Although these events in the Juno era have been reported (e.g. Gershman et al., 2017; Hospodarsky et al., 2017; Vogt et al., 2020), their researches were confined to limited orbits. In this study, we did not remove the fluctuations explicitly from the magnetic data and the updated models are possibly biased by them. The fluctuations associated with the reconnections and/or the magnetopause can be defined by derivations from the updated magnetospheric field models. One of the future works of this study is detection and removal of them using the updated models as the first order approximation. The detection of the events leads to further understanding of the magnetospheric dynamics, and the removal of them will result in reconstruction of both models with more precision.

Europa, Ganymede and Callisto are covered with ice and possible presence of subsurface oceans has been argued (Jia et al., 2010). One of the methods to investigate them is the EM induction method. The electrical structure of the icy moons can be estimated by subtracting the predicted external field (magnetospheric plus intrinsic) from the data and taking ratios of the induced to the external fields. Figure 3 shows hodograms of the magnetic field around each Galilean satellite using JRM09 and our magnetospheric field of the Juno era. Each satellite feels periodic magnetic variations caused by Jupiter's rotation and satellite's revolution. Figure 3 indicates that the Jovian intrinsic field is dominant at Io and Europa because of their proximity to Jupiter, while the magnetospheric field is dominant at Callisto, the farthest Galilean satellite from Jupiter, and comparable at Ganymede. The magnetospheric field, therefore, also plays an important role in the subsurface ocean investigations by the EM induction method. In the near future, two spacecraft missions, JUICE targeting Ganymede and Europa Clipper targeting Europa, will be carried out. It is expected that long-term continuous magnetic field data on satellite-centric orbits will be provided, whose interpretation in terms of the EM induction method can be conducted with the help of the updated models of this study.

7 Summary

In this study, we started with updating the CS shape by following Khurana (1992). The new data by Galileo and Juno in addition to the legendary data by Voyager 1/2 were used. The three models (pre-Galileo, Galileo and Juno) can represent two features of the CS, i.e., bendback and hinge. We found the weak bendback in the Galileo model and the weak hinge in the Juno model. The former can be interpreted as a signature of increased Alfvén velocity in the magnetosphere. Although further investigations on both plasma and orbital effects (e.g., an analysis using spatially binned data) are necessary, the result may imply that there are long-term variations of the magnetic field as well as the plasma environment in the magnetosphere. The latter can be attributed to the weak dynamic pressure of the solar wind in the Juno era. Although it is not clear whether the relatively low CS heights of the other models are biased by spacecraft's trajectories, it may be a good example showing the close coupling between the solar wind and the Jovian magnetosphere.

We also updated the magnetospheric field model by following Khurana (1997). The derived models fit the data well and the fluctuations by magnetic reconnections or magnetopause crossings were found in the data as the deviations from the updated models. Detections of those deviations using the updated models are important to understand the dynamics of the Jovian magnetosphere and to re-update the models with more precision. Being combined with the Jovian intrinsic field model, the magnetospheric field models can be used to predict temporal variations of the magnetic field at each Galilean satellite for EM induction studies. New spacecraft missions, JUICE and Europa Clipper, are planned and the models updated by this study will be of use for the future investigations by new probes.

11

Open Research

The magnetic field data of Voyager 1 (https://pds-ppi.igpp.ucla.edu/search/view/?f=yes&id=pds://PPI/vg1-mag-jup/data-s3coords-48sec), Voyager 2 (https://pds-ppi.igpp.ucla.edu/search/view?f=yes&id=pds://PPI/VJ-MAG-4-SUMM-S3COORDS-48.0SEC-V1.1), Galileo (https://pds-ppi.igpp.ucla.edu/search/view?f=yes&id=J-MAG-3-RDR-MAGSPHERIC-SURVEY-V1.0) and Juno (https://pds-ppi.igpp.ucla.edu/data/JNO-J-3-FGM-CAL-V1.0/) are available from NASA's Planetary Data System.

References

Alexeev, I. I., & Belenkaya, E. S. (2005). Modeling of the Jovian magnetosphere. *Annales Geophysicae*, *23*(3), 809–826. https://doi.org/10.5194/angeo-23-809-2005

Bridge, H. S., Belcher, J. W., Lazarus, A. J., Sullivan, J. D., McNutt, R. L., Bagenal, F., et al. (1979). Plasma observations near Jupiter: Initial results from Voyager 1. *Science*, *204*(4396), 987–991. https://doi.org/10.1126/science.204.4396.987

Connerney, J. E. P. (1992). Doing more with Jupiter's magnetic field. In H. O. Rucker, S. J. Bauer, & M. L. Kaiser (Eds.), *Planetary radio emissions III* (pp. 13–33). Vienna: Austrian Academy of Sciences Press.

Connerney, J. E. P. (2007). Planetary magnetism. In G. Schubert (Eds.), *Treatise on geophysics* (Vol. 10, pp. 243–280). Oxford: Elsevier.

Connerney, J. E. P., Acuña, M. H., & Ness, N. F. (1981). Modeling the Jovian current sheet and inner magnetosphere. *Journal of Geophysical Research: Space Physics*, *86*(A10), 8370–8384. https://doi.org/10.1029/JA086iA10p08370

Connerney, J. E. P., Acuña, M. H., Ness, N. F., & Satoh, T. (1998). New models of Jupiter's magnetic field constrained by the Io flux tube footprint. *Journal of Geophysical Research: Space Physics*, *103*(A6), 11,929–11,939. https://doi.org/10.1029/97JA03726

Connerney, J. E. P., Kotsiaros, S., Oliversen, R. J., Espley, J. R., Joergensen, J. L., Joergensen, P. S., et al. (2018). A new model of Jupiter's magnetic field from Juno's first nine orbits. *Geophysical Research Letters*, *45*(6), 2590–2596. https://doi.org/10.1002/2018GL077312

Connerney, J. E. P., Timmins, S., Herceg, M., & Joergensen, J. L. (2020). A Jovian magnetodisc model for the Juno era. *Journal of Geophysical Research: Space Physics*, *125*(10), e2020JA028138. https://doi.org/10.1029/2020JA028138

Connerney, J. E. P., Timmins, S., Oliverson, R. J., Espley, J. R., Joergensen, J. L., Kotsiaros, S., et al. (2021). A new model of Jupiter's magnetic field at the completion of Juno's prime mission. *Journal of Geophysical Research: Planets*, *127*(2), e2021JE007055. https://doi.org/10.1029/2021JE007055

Gershman, D. J., DiBraccio, G. A., Connerney, J. E. P., Hospodarsky, G., Kurth, W. S., Ebert, R. W., et al. (2017). Juno observations of large-scale com-

pressions of Jupiter's dawnside magnetopause. *Geophysical Research Letters*, *44*(15), 7559–7568. https://doi.org/10.1002/2017GL073132

Gurnett, D. A., Scarf, F. L., Kurth, W. S., Shaw, R. R., & Poynter, R. L. (1981). Determination of Jupiter's electron density profile from plasma wave observations. *Journal of Geophysical Research: Space Physics*, *86*(A10), 8199–8212. https://doi.org/10.1029/JA086iA10p08199

Hess, S. L. G., Bonfond, B., Zarka, P., & Grodent, D. (2011). Model of the Jovian magnetic field topology constrained by the Io auroral emissions. *Journal of Geophysical Research: Space Physics*, *116*(A5). https://doi.org/10.1029/2010JA016262

Hospodarsky, G. B., Kurth, W. S., Bolton, S. J., Allegrini, F., Clark, G. B., Connerney, J. E. P., et al. (2017). Jovian bow shock and magnetopause encounters by the Juno spacecraft. *Geophysical Research Letters*, *44*(10), 4506–4512. https://doi.org/10.1002/2017GL073177

Jackman, C. M., & Arridge, C. S. (2011). Solar cycle effects on the dynamics of Jupiter's and Saturn's magnetospheres. *Solar Physics*, *274*, 481–502. https://doi.org/10.1007/s11207-011-9748-z

Jia, X., Kivelson, M. G., Khurana, K. K., & Walker, R. J. (2010). Magnetic fields of the satellites of Jupiter and Saturn. *Space Science Reviews*, *152*, 271–305. https://doi.org/10.1007/s11214-009-9507-8

Joy, S. P., Kivelson, M. G., Walker, R. J., Khurana, K. K., Russell, C. T., & Ogino, T. (2002). Probabilistic models of the Jovian magnetopause and bow shock locations. *Journal of Geophysical Research: Space Physics, 107*(A10), SMP 17-1-SMP 17-17.

Khurana, K. K. (1992). A generalized hinged-magnetodisc model of Jupiter's nightside current sheet. *Journal of Geophysical Research: Space Physics*, *97*(A5), 6269–6276. https://doi.org/10.1029/92JA00169

Khurana, K. K. (1997). Euler potential models of Jupiter's magnetospheric field. *Journal of Geophysical Research: Space Physics*, *102*(A6), 11,29–11,306. https://doi.org/10.1029/97JA00563

Khurana, K. K. (2001). Influence of solar wind on Jupiter's magnetosphere deduced from currents in the equatorial plane. *Journal of Geophysical Research: Space Physics*, *106*(A11), 25,999–26,016. https://doi.org/10.1029/2000JA000352

Khurana, K. K., & Kivelson, M. G. (1989). On Jovian plasma sheet structure. *Journal of Geophysical Research: Space Physics*, *94*(A9), 11,791–11,803. https://doi.org/10.1029/JA094iA09p11791

Khurana, K. K., Kivelson, M. G., Hand, K. P., & Russell, C. T. (2009). Electromagnetic induction from Europa's ocean and the deep interior. In R. T. Pappalardo, W. B. McKinnon, & K. Khurana (Eds.), *Europa* (pp. 571–586). Tucson: University of Arizona Press.

Khurana, K. K., & Schwarzl, H. K. (2005). Global structure of Jupiter's magnetospheric current sheet. *Journal of Geophysical Research: Space Physics*, *110*(A7). https://doi.org/10.1029/2004JA010757

Kivelson, M. G., Khurana, K. K., Russell, C. T., Walker, R. J., Coleman, P. J., Coroniti, F. V., et al. (1997). Galileo at Jupiter: Changing states of the magnetosphere and first looks at Io and Ganymede. *Advances in Space Research*, *20*(2), 193–204. https://doi.org/10.1016/S0273-1177(97)00533-4

Lanzerotti, L. J., Maclennan, C. G., Krimigis, S. M., Armstrong, T. P., Behannon, K., & Ness, N. F. (1980). Statics of the nightside Jovian plasma sheet. *Geophysical Research Letters*, *7*(10), 817–820. https://doi.org/10.1029/GL007i010p00817

Lorch, C. T. S., Ray, L. C., Arridge, C. S., Khurana, K. K., Martin, C. J., & Bader, A. (2020). Local time asymmetries in Jupiter's magnetodisc currents. *Journal of Geophysical Research*, *125*(2), e2019JA027455. https://doi.org/10.1029/2019JA027455

Moore, K. M., Cao, H., Bloxham, J., Stevenson, D. J., Connerney, J. E. P., & Bolton, S. J. (2019). Time variation of Jupiter's internal magnetic field consistent with zonal wind advection. *Nature Astronomy*, *3*, 730–735. https://doi.org/10.1038/s41550-019-0772-5

Ness, N. F., Acuna, M. H., Lepping, R. P., Burlaga, L. F., Behannon., K. W., & Neubauer, F. M. (1979). Magnetic field studies at Jupiter by Voyager 2: Preliminary results. *Science*, *206*(4421), 966–972. https://doi.org/10.1126/science.206.4421.966

Northrop, T. G., Goertz, C. K., & Thomsen, M. F. (1974). The magnetosphere of Jupiter as observed with Pioneer 10: 2. Nonrigid rotation of the magnetodisc. *Journal of Geophysical Research*, *79*(25), 3579–3582. https://doi.org/10.1029/JA079i025p03579

Ridley, V. A., & Holme, R. (2016). Modeling the Jovian magnetic field and its secular variation using all available magnetic field observations. *Journal of Geophysical Research: Planets*, *121*(3), 309–337. https://doi.org/10.1002/2015JE004951

Russell, C. T., Yu, Z. J., Khurana, K. K., & Kivelson, M. G. (2001). Magnetic field changes in the inner magnetosphere of Jupiter. *Advances in Space Research*, *28*(6), 897–902. https://doi.org/10.1016/S0273-1177(01)00513-0

Smith, E. J., Davis, L., Jr., Jones, D. E., Coleman, P. J., Jr., Colburn, D. S., Dyal, P., et al. (1974). The planetary magnetic field and magnetosphere of Jupiter: Pioneer 10. *Journal of Geophysical Research*, *79*(25), 3501–3513. https://doi.org/10.1029/JA079i025p03501

Stern, D. P. (1970). Euler potentials. *American Journal of Physics*, *38*(4), 494–501. https://doi.org/10.1119/1.1976373

Stern, D. P. (1976). Representation of magnetic fields in space. *Reviews of Geophysics*, *14*(2), 199–214. https://doi.org/10.1029/RG014i002p00199

Van Allen, J. A., Baker, D. N., Randall, B. A., Thomsen, M. F., Sentman, D. D., & Flindt, H. R. (1974). Energetic electrons in the magnetosphere of Jupiter. *Science*, *183*(4122), 309–311. https://doi.org/10.1126/science.183.4122.309

Vogt, M. F., Bunce, E. J., Nichols, J. D., Clarke, J. T., & Kurth, W. S. (2017). Long-term variability of Jupiter's magnetodisk and implications for the aurora. *Journal of Geophysical Research: Space Physics*, *122*(12), 12,090–12,110. https://doi.org/10.1002/2017JA024066

Vogt, M. F., Connerney, J. E. P., DiBraccio, G. A., Wilson, R. J., Thomsen, M. F., Ebert, R. W., et al. (2020). Magnetotail reconnection at Jupiter: A survey of Juno magnetic field observations. *Journal of Geophysical Research: Space Physics*, *125*(3), e2019JA027486. https://doi.org/10.1029/2019JA027486

Wang, J., Huo, Z., & Zhang, L. (2022). An empirical model of the current sheet in Jupiter's magnetosphere. *Planetary and Space Science*, *211*, 105395. https://doi.org/10.1016/j.pss.2021.105395

Yu, Z. J., Leinweber, H. K., & Russell, C. T. (2010). Galileo constraints on the secular variation of the Jovian magnetic field. *Journal of Geophysical Research: Planets*, *115*(E3). https://doi.org/10.1029/2009JE003492

Geophysical Research Letters

Supporting Information for

Updated Models of Current Sheet and Magnetic Field in the Jovian Magnetosphere for Pre-Galileo, Galileo and Juno Eras

Naoya Momoki[1] and Hiroaki Toh[2]

[1] Division of Earth and Planetary Sciences, Graduate School of Science, Kyoto University

[2] Data Analysis Center for Geomagnetism and Space Magnetism, Graduate School of Science, Kyoto University

Contents of this file

Introduction

This supplement provides two additional descriptions about the CS shape and magnetospheric filed model parameters and eight figures in order to show the detailed characteristics of the models updated in this study. The additional texts describe the parameterization of the two models and meaning of the model parameters. Text 1 is for the CS shape model, and Text 2 is for the magnetospheric field model. The current sheet has two characteristics as mentioned in the main text, namely, bendback and hinge. Figure S1 represents comparison of the bendback effect with δ in Eq. (1). Figure S2 represents comparison of the hinge effect in the midnight meridional plane where the effect becomes most prominent. Figure S3 shows the comparison of the magnetospheric field model parameters among the three models (pre-Galileo, Galileo, and Juno) with parameter error estimates based on the observation errors. Figures S4 through S6 indicate the stability of the updated magnetospheric field model by showing the RMS curves in the vicinity of the optimized parameters listed in Table 1 of the main text. These figures are for pre-Galileo, Galileo and Juno, respectively. Figures S7 and S8 represent the calculated azimuthal electric current density using the field models updated in this study for Galileo and Juno, respectively.

Text S1.

In this text, the CS shape model parameters (x_0, ρ_0, v_0) are described in detail.

The x_0 controls the hinge effect mentioned in the main text through the term in Eq. (1):

$$\rho \frac{x_0}{x} \tanh\left(\frac{x}{x_0}\right). \tag{S1}$$

First, considering the dawn-dusk meridian, $x = 0$ and $\rho = |y|$, which is dusk-directional distance on the equatorial plane. In the case of $|x| \ll |x_0|$, by using an approximation,

$$\tanh\left(\frac{x}{x_0}\right) \simeq \frac{x}{x_0}, \tag{S2}$$

the term (S1) becomes a simpler form:

$$\rho \frac{x_0}{x} \tanh\left(\frac{x}{x_0}\right) \simeq |y| \ . \tag{S3}$$

The CS shape model (1), therefore, can be simplified:

$$Z_{CS} \simeq |y| \tan(\theta_d) \cos(\lambda - \delta). \tag{S4}$$

This means that the Z-coordinate of the CS is not constrained by ρ in this meridian. Next, on the midnight meridian where $\rho = -x$, the CS shape model (1) becomes

$$Z_{CS} = -\tan(\theta_d)\, x_0 \tanh\left(\frac{x}{x_0}\right) \cos(\lambda - \delta). \tag{S5}$$

While in the case of $|x| \ll |x_0|$ (i.e. near Jupiter), (S5) can be simplified to the same form as (S4):

$$Z_{CS} \simeq -x \tan(\theta_d) \cos(\lambda - \delta) \ , \tag{S6}$$

in the case of $|x| \gg |x_0|$ (i.e., distant from Jupiter), the hyperbolic tangent term becomes unity and the Z-coordinate of the CS is independent of ρ:

$$Z_{CS} = -\tan(\theta_d)\, x_0 \cos(\lambda - \delta) \ . \tag{S7}$$

This means the Z-coordinate is saturated with large x, and x_0 is the scale distance where the hinge effect becomes dominant and rules the maximum height of the CS $(\tan(\theta_d)\,|x_0|)$.

On the other hand, ρ_0 and v_0 control the bendback effect mentioned in the main text through the term:

$$\frac{\Omega_J \rho_0}{v_0} \ln \cosh\left(\frac{\rho}{\rho_0}\right) \ . \tag{S8}$$

While δ in Eq. (1) means the longitude at which the CS has the maximum tilt without

the hinge effect, it isn't equal to the longitude at which the Jupiter's dipole points, λ_d. δ varies as a function of ρ corresponding to the finite propagation velocity of the CS oscillation originated from the rotation of Jupiter's dipole. The difference between the longitudes, therefore, can be formulated in an integral form:

$$\delta - \lambda_d = \Omega_J \int_0^\rho \frac{d\rho}{v(\rho)} \tag{S9}$$

where v is the propagation velocity as the function of ρ. In this model, the velocity is modeled by using the hyperbolic tangent:

$$v(\rho) = \frac{v_0}{\tanh\left(\frac{\rho}{\rho_0}\right)}, \tag{S10}$$

and by integrating it, δ in Eq. (1) can be obtained. In the case of $\rho \ll \rho_0$, $v(\rho)$ diverges to infinity with the approximation (S2), and this corresponds to no bendback effect near Jupiter because of the infinite propagation velocity. In a contrasting situation, $\rho \gg \rho_0$, the velocity reaches a constant value, v_0. It follows that ρ_0 controls the distance where the bendback effect becomes dominant, and v_0 rules the strength of the effect.

Text S2.

In this text, we will explain what the magnetospheric field model parameters means.

The magnetospheric field model is formulated by the Euler potentials f and g that are the functions of the spatial coordinates (ρ_m, ϕ, Z_m):

$$
\begin{aligned}
\boldsymbol{B} &= \nabla f(\rho_m, \phi, Z_m) \times \nabla g(\rho_m, \phi, Z_m), \\
B_{\rho_m} &= \frac{\partial f}{\rho_m \partial \phi} \frac{\partial g}{\partial Z_m} - \frac{\partial f}{\partial Z_m} \frac{\partial g}{\rho_m \partial \phi}, \\
B_\phi &= \frac{\partial f}{\partial Z_m} \frac{\partial g}{\partial \rho_m} - \frac{\partial f}{\partial \rho_m} \frac{\partial g}{\partial Z_m}, \\
B_{Z_m} &= \frac{\partial f}{\partial \rho_m} \frac{\partial g}{\rho_m \partial \phi} - \frac{\partial f}{\rho_m \partial \phi} \frac{\partial g}{\partial \rho_m}.
\end{aligned}
\tag{S11}
$$

The formulation using the Euler potentials was obtained as follows. The observed B_{ρ_m} and B_{Z_m} were well explained by their zeroth-order approximations (Khurana, 1997), $B_{\rho_m 0}$ and $B_{Z_m 0}$:

$$
\begin{aligned}
B_{\rho_m 0} &= C_1 \left\{ \tanh\left(\frac{\rho_{01}}{\rho_m}\right) \right\}^{a_1} \tanh\left(\frac{Z_m}{D_1}\right), \\
B_{Z_m 0} &= C_2 \left\{ \tanh\left(\frac{\rho_{02}}{\rho_m}\right) \right\}^{a_2} + C_3 \left\{ \tanh\left(\frac{\rho_{03}}{\rho_m}\right) \right\}^{a_3} + C_4.
\end{aligned}
\tag{S12}
$$

Assuming a Euler potential g_0, the zeroth-order approximation of the g, is equal to ϕ, $B_{\rho_m 0}$, $B_{Z_m 0}$, and $B_{\phi 0}$ (the zeroth-order approximation of the B_ϕ) can be expressed by f_0, the zeroth-order approximation of the f:

$$
\begin{aligned}
B_{\rho_m 0} &= -\frac{1}{\rho_m}\frac{\partial f_0}{\partial Z_m}, \\
B_{\phi 0} &= 0, \\
B_{Z_m 0} &= \frac{1}{\rho_m}\frac{\partial f_0}{\partial \rho_m}.
\end{aligned}
\tag{S13}
$$

Using (S12) and (S13), f_0 can be obtained:

$$
\begin{aligned}
f_0 &= -\int \rho_m B_{\rho_m 0}\, dZ_m + \int \rho_m B_{Z_m 0}\, d\rho_m \\
&= -C_1 \rho_m \left\{ \tanh\left(\frac{\rho_{01}}{\rho_m}\right) \right\}^{a_1} \ln\cosh\left(\frac{Z_m}{D_1}\right) \\
&\quad + \int \rho_m \left\{ C_2 \left\{ \tanh\left(\frac{\rho_{02}}{\rho_m}\right) \right\}^{a_2} + C_3 \left\{ \tanh\left(\frac{\rho_{03}}{\rho_m}\right) \right\}^{a_3} + C_4 \right\} d\rho_m.
\end{aligned}
\tag{S14}
$$

where the term $C_1 D_1$ emerged by the integration is redefined as the C_1. In Khurana (1997), Z_m was modified to $Z_m - Z_{m,CS}$ corresponding to the complex shape of the current sheet, and ρ_{01}/ρ_m was replaced by r_{01}/r.

The parameter C_1 (more precisely, C_1/D_1) and C_2 through C_4 represent the B_ρ and the components of the B_{Z_m} at $\rho_m = 0$. Furthermore, considering the approximation of the hyperbolic tangent (S2) where $\rho_m \gg \rho_0$, a_1 through a_3 represent the powers with which each component decreases, and r_{01}, ρ_{02}, and ρ_{03} represent the scale distances where the power law become significant. D_1 is regarded as the Z_m-directional distance where the B_{ρ_m} is saturated with increasing $Z_m - Z_{m,CS}$.

g can be obtained by adding the bendback effect of the magnetic field to the g_0 and it is formulated as the second term of Eq. (2). Considering the typical values of the p and q are both positive, the term increases and ϕ decreases with increasing ρ_m on a magnetic field line in order to conserve the Euler potential g. The parameters p, q, and D_2 are regarded as the bendback rate against ρ_m at the center of the CS, the increment of the bendback rate with increasing $Z_m - Z_{m,CS}$, and the Z_m-directional distance where the effect of q is saturated.
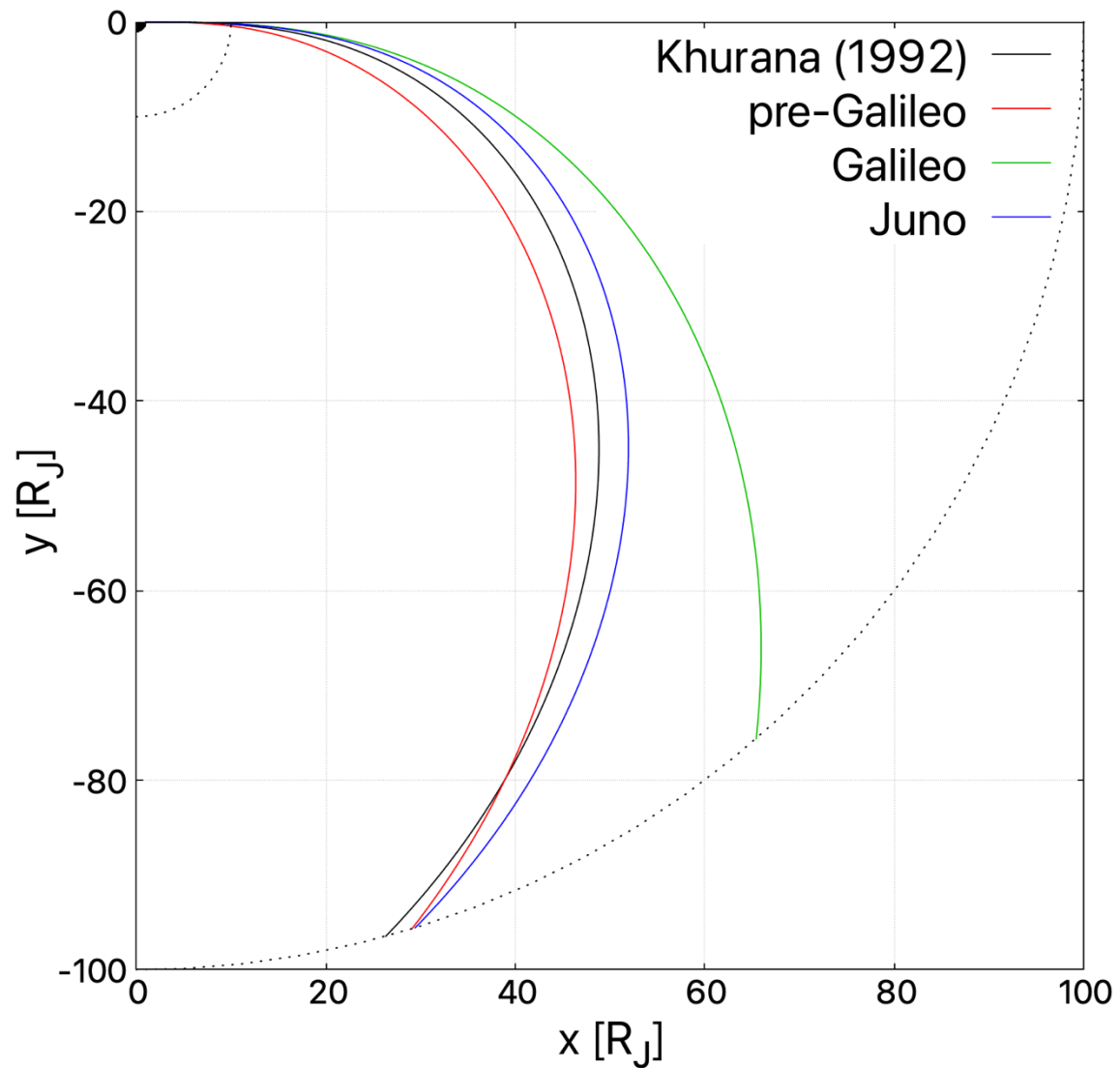
Figure S1. Comparison of the bendback effect of the CS shape models on the Jovigraphical equatorial plane with the System III longitude $\lambda = \lambda_d$ as x-axis. The x and y distances are measured in units of R_J. Each curve represents the modeled δ of Khurana (1992) (black), pre-Galileo (red), Galileo (green) and Juno (blue). The black area at the origin represents Jupiter and the two dotted circles represent the distance range of the used data (10 R_J and 100 R_J from the origin, respectively).
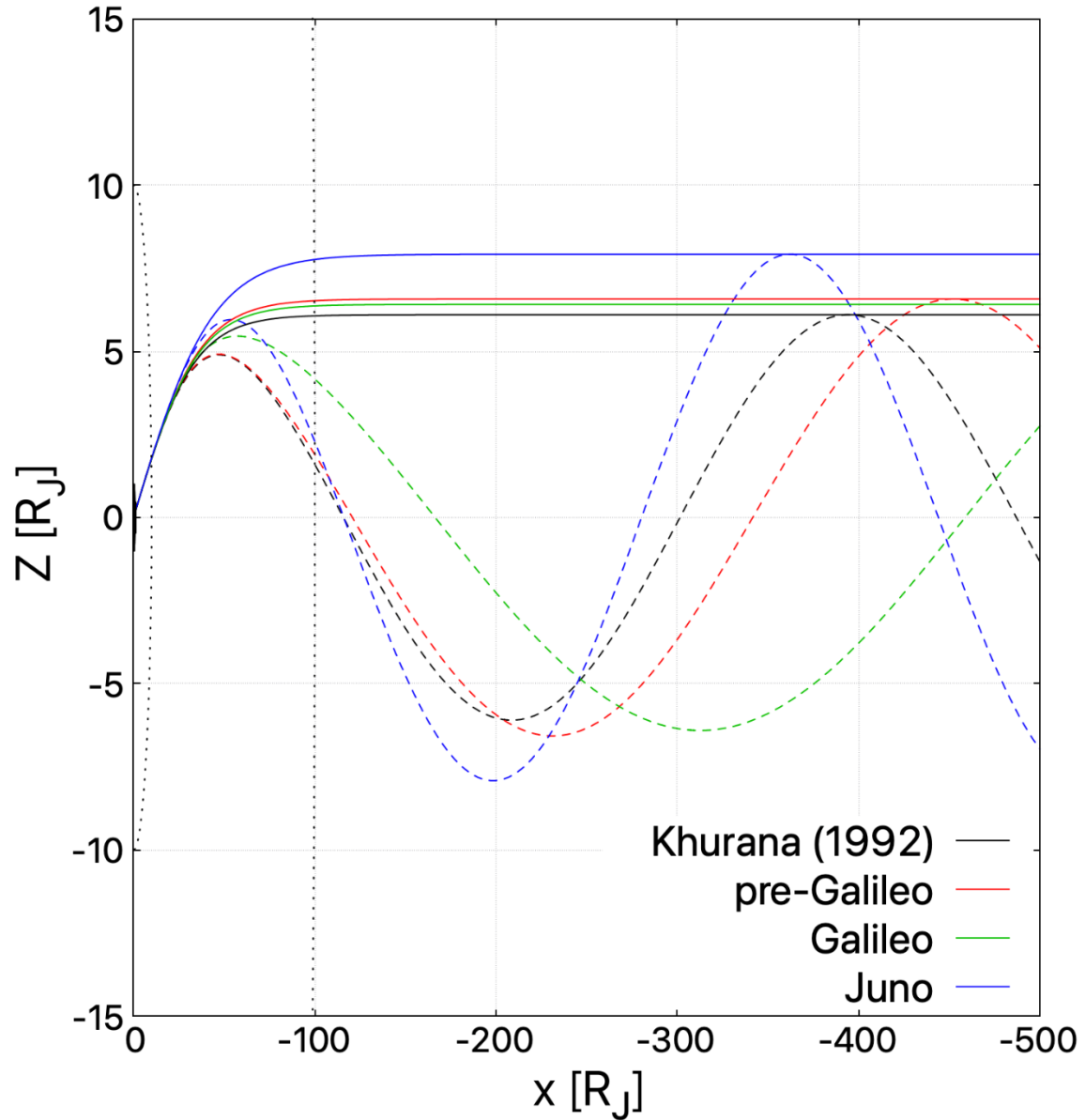
Figure S2. Comparison of the hinge effect of the CS shape models in the Jovigraphical midnight meridional plane whose distances are measured in R_J with sunward direction as x-axis. Dashed curves represent cross-sections of the CSs in the midnight meridian whose System III longitude λ is λ_d, while solid curves denote those in the pseudo prime meridian ($\lambda = \delta$) at midnight. The colors corresponding to the models are the same as Figure S1. Black dotted curves represent the distance range of the used data.
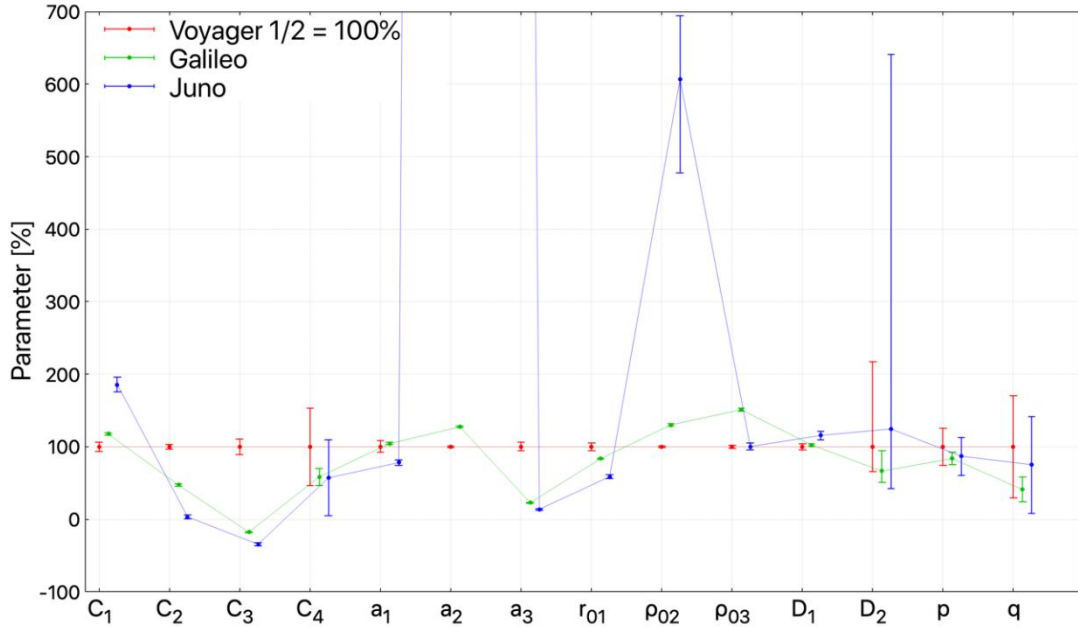
Figure S3. The updated parameters normalized by each pre-Galileo parameter and their estimated errors. Red, blue and green parameters represent those in pre-Galileo (Voyager 1/2), Galileo and Juno models, respectively. The errors are estimated based on the errors of the observed magnetic field.
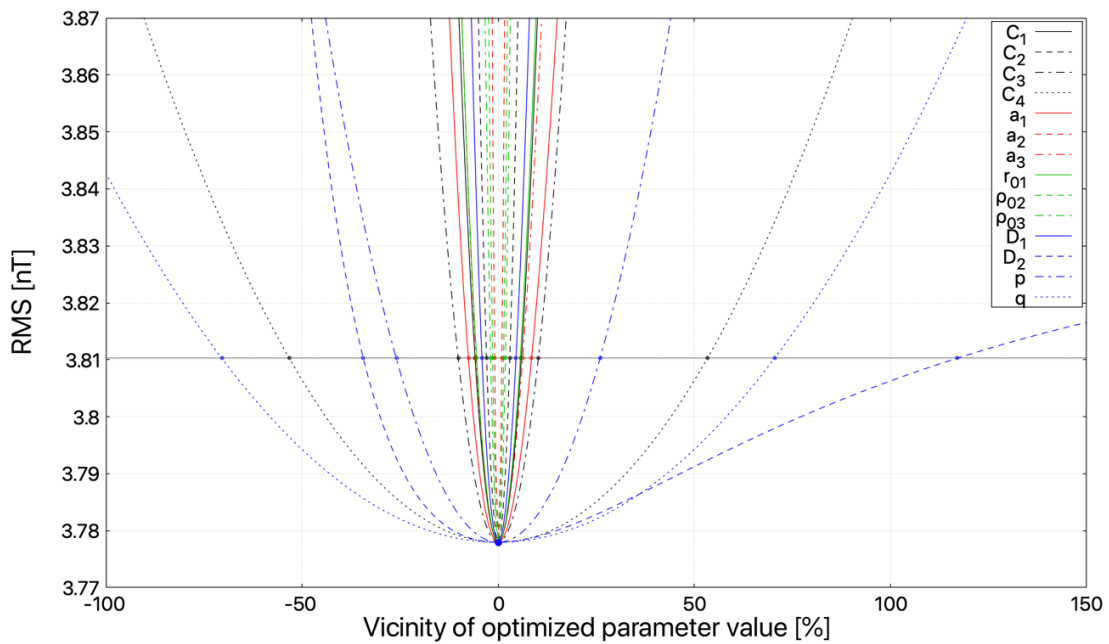

Figure S4. The RMS distributions in the vicinity of each updated magnetospheric model parameter in the pre-Galileo era listed in Table 1. The horizontal line represents the possible RMS value when the observation errors are considered, and the cross points with each curve correspond to each error bar in the Figure S3.
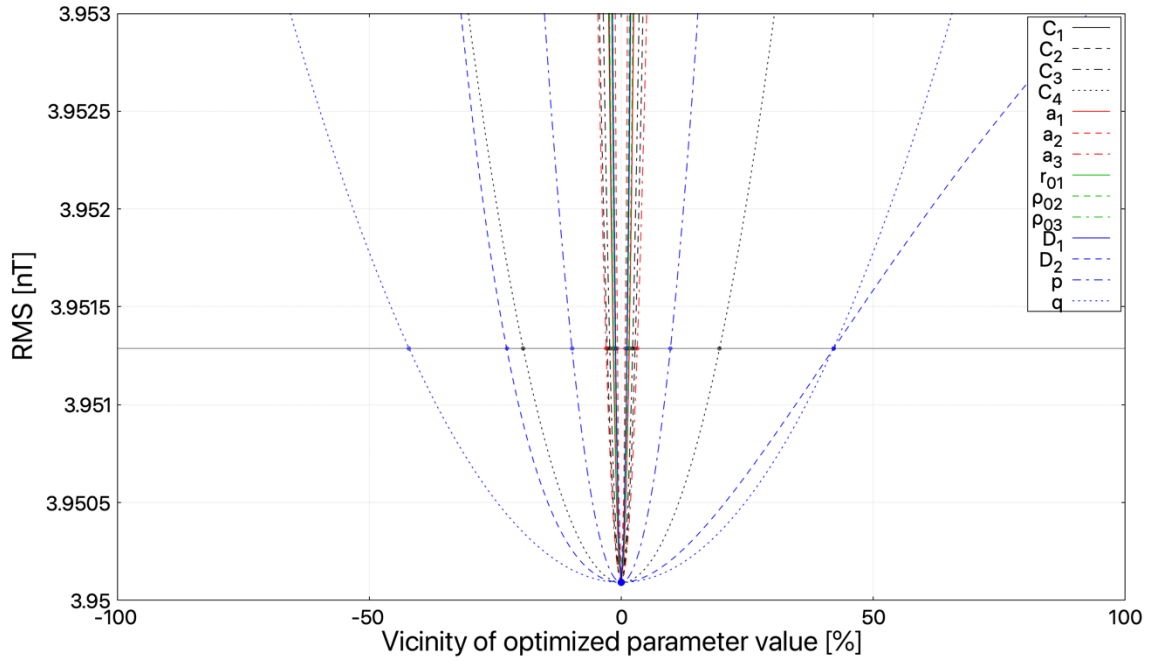
Figure S5. The RMS distributions in the vicinity of each updated magnetospheric model parameter in the Galileo era listed in Table 1. The figure format is same as Figure S4.
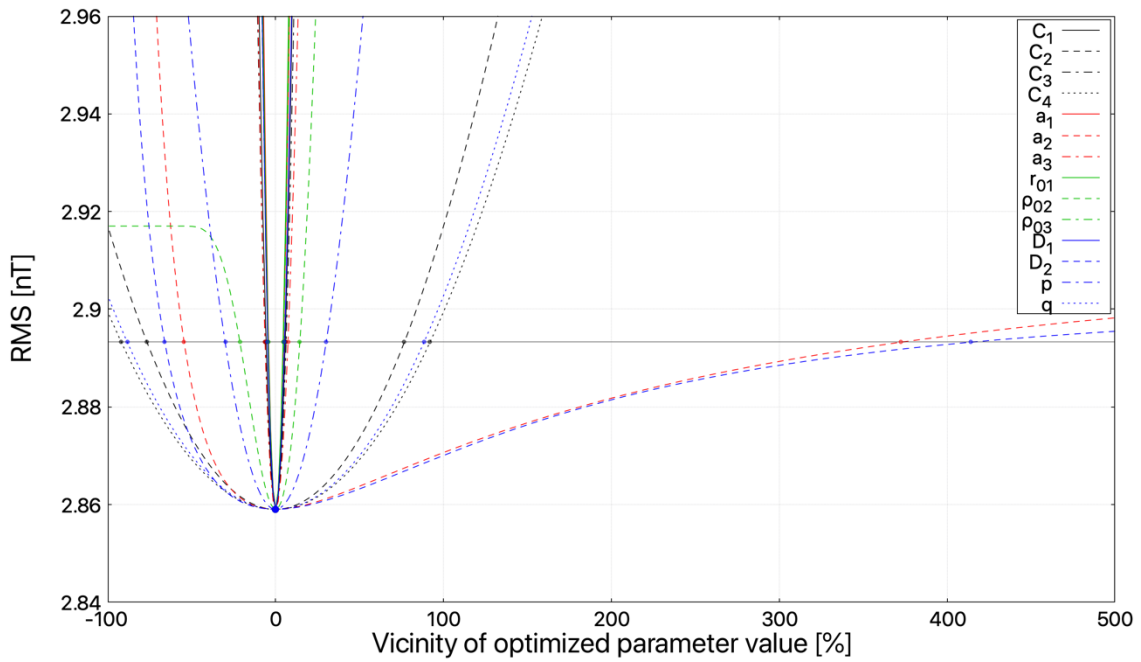

Figure S6. The RMS distributions in the vicinity of each updated magnetospheric model parameter in the Juno era listed in Table 1. The figure format is same as Figure S4.
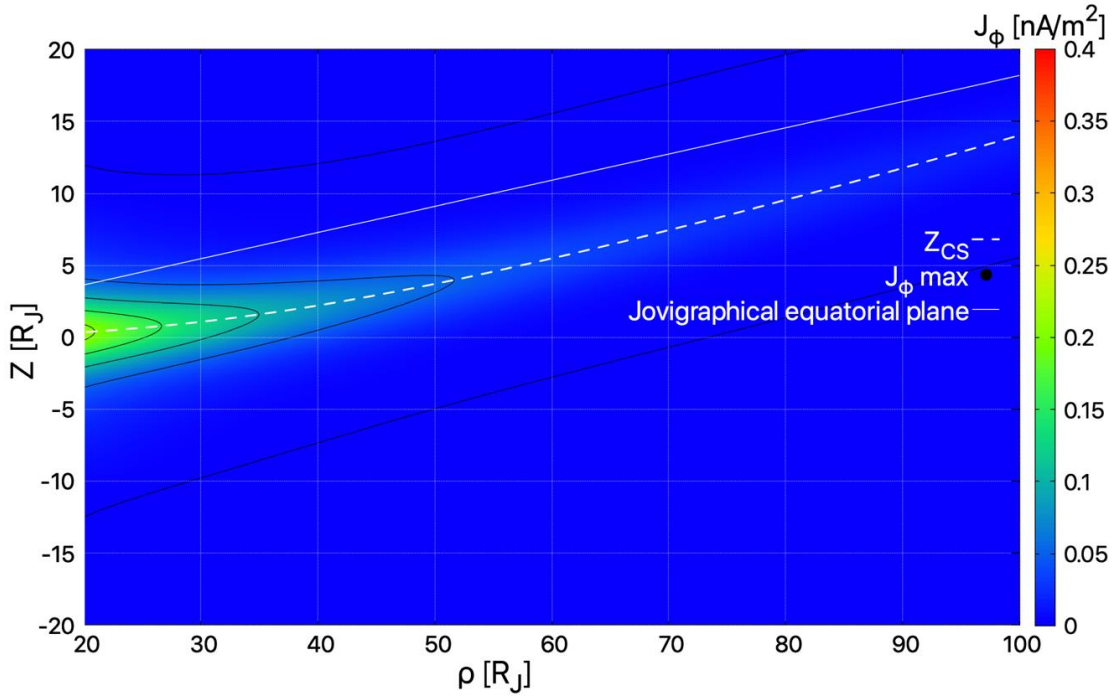
Figure S7. The azimuthal electric current density calculated by the updated magnetospheric field model in the Galileo era on the midnight meridian using the magnetic dipole coordinate system. The solid and dashed white lines represent the cross-sections of the Jovigraphical equator and modeled CS on this meridian.
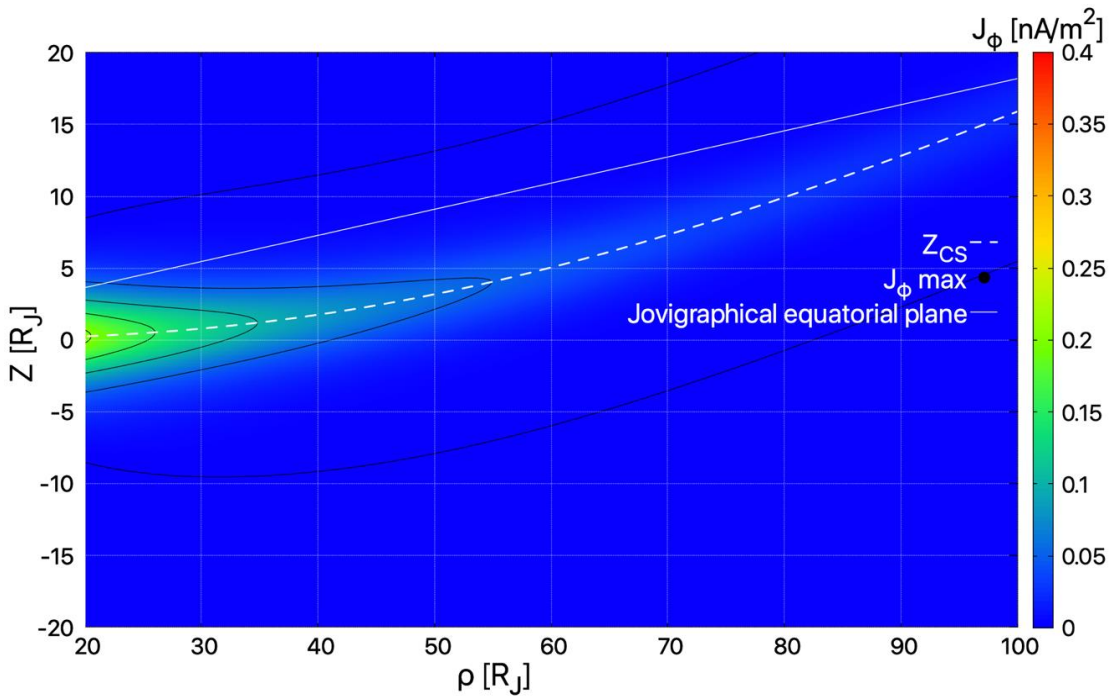

Figure S8. The azimuthal electric current density calculated by the updated magnetospheric field model in the Juno era. The figure format is same as Figure S7.